

# Separation detection and correction of mosaic errors in mosaic gratings based on two detection lights with the same diffraction order and different incident angles



Guojun Yang<sup>a,b</sup>, Xiangdong Qi<sup>a,\*</sup>, Xiaotao Mi<sup>a,\*</sup>, Shanwen Zhang<sup>a</sup>, Hongzhu Yu<sup>a</sup>, Haili Yu<sup>a</sup>, Xiaotian Li<sup>a</sup>

<sup>a</sup> Changchun Institute of Optics, Fine Mechanics and Physics, Chinese Academy of Sciences, No. 3888 Dong Nanhu Road, Changchun, Jilin 130033, China  
<sup>b</sup> University of Chinese Academy of Sciences, Beijing 100049, China

## ARTICLE INFO

**Keywords:**  
 Grating tiling  
 Mosaic errors  
 Separation detection  
 Measurement uncertainty  
 Mosaic accuracy

## ABSTRACT

Grating tiling is an important fabrication technology for large-size gratings. However, when using grating tiling technology to form large-size echelle gratings, the interferometer cannot detect the grating's zero-order diffraction wavefront because the zero-order diffraction light of the echelle grating is weak. This prevents use of the zero-order and non-zero-order diffraction light of the grating to realize separation detection and correction of mosaic errors. To solve this problem, a new method for separation detection and correction of mosaic errors in mosaic gratings based on two detection lights with the same diffraction order but different incident angles is proposed and a mosaic error detection system is designed. Then, the correction steps for mosaic errors are summarized and the error in mosaic error detection system is analyzed. Finally, the measurement uncertainty in detecting the wavefront of the mosaic grating and the mosaic accuracy of the grating wavefront are analyzed. The uncertainty is  $0.008\lambda$  ( $\lambda=632.8\text{ nm}$ ) and the mosaic accuracy of the peak-to-valley wavefront is  $0.069\lambda$ , which shows that high-precision measurements of the wavefront and high-precision mosaic of the wavefront were successfully achieved. The proposed method can be used for the mosaic of all blazed gratings.

## 1. Introduction

Diffraction gratings have been widely used as optical elements in applications including spectrometers [1–3], lasers [4–6], and couplers [7–9]. Among these applications, astronomical spectrometers and nuclear fusion laser systems need to be equipped with large-size diffraction gratings to meet the spectrometer's requirements for high resolution and the laser's requirements for high energy. Spectrometers such as the GMT-Consortium Large Earth Finder (G-CLEF) [10] and ESPRESSO [11] and laser systems such as OMEGA EP [12] and PETAL [13] are all equipped with large-size diffraction gratings. In light of the difficulty of fabricating single large-size diffraction gratings, grating tiling technology was proposed. Grating tiling technology involves placing two or more relatively small-sized gratings together, adjusting their attitudes and their relative positional relationships, and then rectifying the five dimensional errors until their error tolerance requirements are met. The core process of the grating tiling technique is the separation detection and correction of mosaic errors.

In 2007, based on the far-field diffraction principle, Yang et al. realized the separation detection and correction of rotation errors using

zero-order and diffraction-order light of a single wavelength and also realized the separation detection and correction of translation errors using a Michelson interferometer [14]. Zeng et al. realized the separation detection and correction of rotation errors using zero-order and diffraction-order light of a single wavelength and realized the separation detection and correction of translation errors using diffraction-order light with dual wavelengths [15–17]. However, Qiao et al. analyzed the far-field pattern and the near-field diffraction wavefront and concluded that there was aberration in the far-field imaging system for large-aperture beams. This aberration would lead to inconsistency between the mosaic errors reflected by the mosaic wavefront and the measured far-field pattern. The optimal far-field pattern quality thus did not correspond to the optimal mosaic state. The mosaic quality is better reflected by all mosaicked grating wavefronts in the near field [18].

Therefore, in 2016, based on the interference principle, Lu et al. realized the separation detection and correction of the five dimensional mosaic errors using zero-order diffraction light and non-zero-order diffraction light of a single wavelength [19]. However, based on the interference principle, the mosaic error is detected and corrected using the zero-order and non-zero-order diffraction light of the grating, which is

\* Corresponding authors.

E-mail addresses: [chinagrating@263.net](mailto:chinagrating@263.net) (X. Qi), [mixiaotao\\_ciomp@126.com](mailto:mixiaotao_ciomp@126.com) (X. Mi).

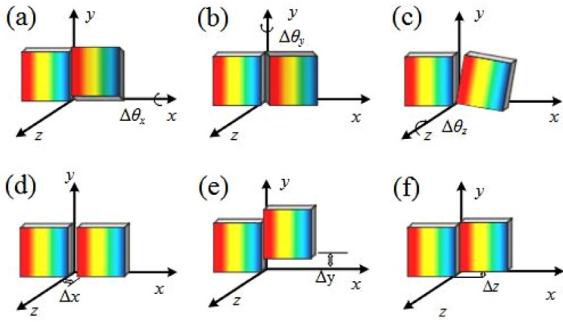


**Fig. 1.** Mosaic errors between mosaic gratings. The  $x$ -axis is parallel to the grating vector direction, the  $y$ -axis is parallel to the grating line direction, and the  $z$ -axis is parallel to the grating normal direction.

only suitable for a mosaic of ordinary blazed gratings and is not suitable for a mosaic of echelle gratings with weak zero-order diffraction light. Therefore, to solve the problem that the zero-order diffraction light of the echelle grating cannot be used to complete the separation detection and correction of the mosaic errors, in 2018, Cong et al. proposed reservation of a specific area of the aluminum film on the edge of the mosaic grating; they then used the light reflected by the aluminum film rather than the zero-order diffraction light of the echelle grating at the same angle of incidence to detect and correct mosaic errors [20,21]. However, the effective area of the mosaic gratings is much smaller than that of the larger aluminum film. Additionally, the mosaic errors will not be completely corrected if a smaller aluminum film is used because the surface shape of the aluminum film area is insufficient to characterize the surface shape of the grating area. Therefore, the separation detection of mosaic errors should mainly focus on detection of the grating area.

To solve the problem of error separation detection and correction in mosaicking echelle gratings, we propose a new five dimensional mosaic error separation detection and correction method for all blazed gratings. In this paper, **Section 2** introduces the method for separation detection and correction of mosaic errors. **Section 3** introduces the mosaic error separation detection system and the correction of the initial errors  $\Delta\theta_x$  and  $\Delta z$ . **Section 4** introduces the results and discussion.

## 2. Method of separation detection and correction of mosaic error

### 2.1. Description of mosaic error

There are six dimensional errors in the mosaicking of two gratings as shown in **Fig. 1**. The six dimensional mosaic errors are listed as follows:  $\Delta\theta_x$ , which is the error of rotation around the  $x$ -axis (grating vector direction), as shown in **Fig. 1(a)**;  $\Delta\theta_y$ , which is the error of rotation around the  $y$ -axis (grating line direction), as shown in **Fig. 1(b)**;  $\Delta\theta_z$ , which is the error of rotation around the  $z$ -axis (grating normal direction), as shown in **Fig. 1(c)**;  $\Delta x$ , which is the error of translation along the  $x$ -axis (grating vector direction), as shown in **Fig. 1(d)**;  $\Delta y$ , which is the error of translation along the  $y$ -axis (grating line direction), as shown in **Fig. 1(e)**; and  $\Delta z$ , which is the error of translation along the  $z$ -axis (grating normal direction), as shown in **Fig. 1(f)**. Among these errors, the translation error  $\Delta y$  only affects the effective area of the mosaic grating and does not affect the mosaic grating performance, so it can be ignored.

According to the grating equation and grating cone diffraction theory, the relationship between the mosaic error and the diffraction wavefront is given by **Eq. (1)** [19]:

$$\Delta_{OPD} = 2 \left\{ (\cos \alpha + \cos \beta) \cdot \frac{\Delta\theta_y}{\cos \beta} \cdot u + \left[ \frac{m\lambda}{d} \cdot \Delta\theta_z - (\cos \alpha + \cos \beta) \cdot \Delta\theta_x \right] \cdot v + \left[ \frac{m\lambda}{d} \cdot \Delta x - (\cos \alpha + \cos \beta) \cdot \Delta z \right] \right\} \quad (1)$$

Where,  $\alpha$  is the incident angle,  $\beta$  is the diffraction angle,  $d$  is the grating constant,  $m$  is the diffraction order, and  $\Delta_{OPD}$  is the optical path difference between the mosaic gratings.

From **Eq. (1)**, the influence of the five dimensional mosaic errors on the grating diffraction wavefront can be analyzed as follows:  $\Delta\theta_y$  can cause the interference fringe of the moving grating tilt to change when compared with the interference fringe of the static grating;  $\Delta\theta_x$  and  $\Delta\theta_z$  can cause the interference fringe of the moving grating width to change when compared with the interference fringe of the static grating; and  $\Delta x$  and  $\Delta z$  can cause the interference fringe of the moving grating displacement to change when compared with the interference fringe of the static grating. According to this analysis, the separation detection and correction of  $\Delta\theta_y$  can be realized based on the tilt difference between the interference fringes of the mosaic grating, but the separation detection and correction of  $\Delta\theta_x$  and  $\Delta\theta_z$  cannot be realized because they will influence each other, and the separation detection and correction of  $\Delta x$  and  $\Delta z$  also cannot be realized because they will influence each other.

### 2.2. Separation detection and correction of mosaic error

To realize the separation detection and correction of  $\Delta\theta_x$  and  $\Delta\theta_z$  and to realize the separation detection and correction of  $\Delta x$  and  $\Delta z$ , we propose to detect and correct the mosaic errors using the same diffraction order for the detection beam but different incident angles. In addition, based on the use of two detection beams with the same diffraction order  $m$  and different incident angles of  $\alpha 1$  and  $\alpha 2$ , the interference fields of two groups of mosaic gratings can be obtained. The interference fields of these two groups of mosaic gratings can be defined as the  $\alpha 1$  interference field and the  $\alpha 2$  interference field.

According to **Eq. (1)**, the relationships between the mosaic error and the diffraction wavefront between the  $\alpha 1$  interference field and the  $\alpha 2$  interference field can be written as follows:

$$\begin{aligned} \Delta(2-1)_{OPD} &= \Delta 2_{OPD} - \Delta 1_{OPD} \\ &= 2 \cdot [(\cos \alpha 1 + \cos \beta 1 - \cos \alpha 2 - \cos \beta 2) \cdot \Delta\theta_x \\ &\quad \cdot v + (\cos \alpha 1 + \cos \beta 1 - \cos \alpha 2 - \cos \beta 2) \cdot \Delta z] \end{aligned} \quad (2)$$

Where,  $\alpha 1$  is the incident angle in the  $\alpha 1$  interference field,  $\alpha 2$  is the incident angle in the  $\alpha 2$  interference field,  $\beta 1$  is the diffraction angle in the  $\alpha 1$  interference field,  $\beta 2$  is the diffraction angle in the  $\alpha 2$  interference field,  $\Delta 1_{OPD}$  is the optical path difference between the mosaic gratings in the  $\alpha 1$  interference field, and  $\Delta 2_{OPD}$  is the optical path difference between the mosaic gratings in the  $\alpha 2$  interference field.

From **Eq. (2)**, the influence of the five dimensional mosaic errors on the grating diffraction wavefront can be analyzed as follows: only  $\Delta\theta_x$  can make the width of the interference fringes of moving gratings in the  $\alpha 1$  interference field change when compared with the interference fringes of moving gratings in the  $\alpha 2$  interference field; only  $\Delta z$  can make the displacement of the interference fringe of the moving grating change in the  $\alpha 1$  interference field when compared with the interference fringe of the moving grating in the  $\alpha 2$  interference field. According to this analysis, the separation detection and correction of  $\Delta\theta_x$  and  $\Delta\theta_z$  can then be realized based on the width difference between the interference fringes of moving gratings in the  $\alpha 1$  and  $\alpha 2$  interference fields, and the width difference between the interference fringes of moving and static gratings in the  $\alpha 1$  or  $\alpha 2$  interference fields, respectively. Additionally, the separation detection and correction of  $\Delta z$  and  $\Delta x$  can be realized based on the displacement difference between the interference fringes of moving gratings in the  $\alpha 1$  and  $\alpha 2$  interference fields and the displacement difference between the interference fringes of moving and static gratings in the  $\alpha 1$  or  $\alpha 2$  interference fields, respectively.

However, based on the order where the rotation error is corrected first and then the translation error is corrected, according to **Eq. (2)**, it is necessary to meet the following requirements when correcting  $\Delta\theta_x$  and  $\Delta z$ :

$$\Delta\theta_x = \frac{\Delta(2-1)_{OPD} - 2 \cdot (\cos \alpha 1 + \cos \beta 1 - \cos \alpha 2 - \cos \beta 2) \cdot \Delta z}{2 \cdot (\cos \alpha 1 + \cos \beta 1 - \cos \alpha 2 - \cos \beta 2) \cdot v} \quad (3)$$

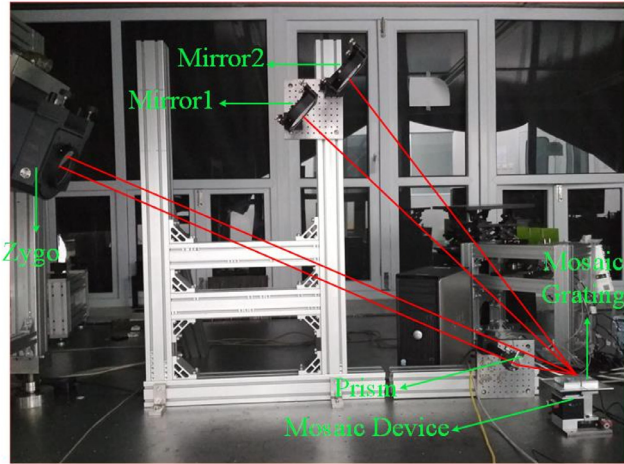


**Fig. 2.** Experimental optical path diagram of separation detection system for mosaic error.

$$\Delta z = \frac{\Delta(2 - 1)_{OPD}}{2 \cdot (\cos \alpha_1 + \cos \beta_1 - \cos \alpha_2 - \cos \beta_2)} \quad (4)$$

Where,  $\Delta(2 - 1)_{OPD} = a\lambda + b\lambda$  ( $a = 0, \pm 1, \pm 2, \dots; 0 \leq b \leq 1$ ). For a perfect mosaic, it is necessary for  $\Delta\theta_x$  to be equal to 0 and  $\Delta z$  to be equal to 0, which means that the parameter  $a$  is equal to 0 and the maximum value of  $b$  is equal to 1. Then, based on Eqs. (3) and (4), the initial values of  $\Delta\theta_x$  and  $\Delta z$  must meet the following requirements when correcting  $\Delta\theta_x$  and  $\Delta z$ :

$$\Delta\theta_x = \frac{\lambda - 2 \cdot (\cos \alpha_1 + \cos \beta_1 - \cos \alpha_2 - \cos \beta_2) \cdot \Delta z}{2 \cdot (\cos \alpha_1 + \cos \beta_1 - \cos \alpha_2 - \cos \beta_2) \cdot v} \quad (5)$$

$$\Delta z = \frac{\lambda}{2 \cdot (\cos \alpha_1 + \cos \beta_1 - \cos \alpha_2 - \cos \beta_2)} \quad (6)$$

Finally,  $\Delta\theta_x$  can be corrected by adjusting the width of the interference fringes of moving gratings in the  $\alpha_1$  interference field when compared with the interference fringes of moving gratings in the  $\alpha_2$  interference field based on the premise that the value of  $\Delta\theta_x$  is less than or equal to that given by Eq. (5). Additionally,  $\Delta z$  can be corrected by adjusting the displacement of the interference fringes of moving gratings in the  $\alpha_1$  interference field when compared with the interference fringes of moving gratings in the  $\alpha_2$  interference field based on the premise that the value of  $\Delta z$  is less than or equal to that given by Eq. (6).

### 3. Experimental

#### 3.1. Mosaic error detection system

To cause the interference fringes of mosaic gratings in the  $\alpha_1$  and  $\alpha_2$  interference fields to appear on the same detector simultaneously and improve the correction accuracy of mosaic errors, a prism is introduced into the error detection optical path to generate a second incident angle for the detection beam in the same error detection optical path, as shown in Fig. 2.

Fig. 2 shows the experimental optical path diagram of the separation detection system for the mosaic error based on the same diffraction order and different incident angles. Here, a Zygo interferometer is used to detect the wavefronts of the mosaic gratings and obtain the mosaic grating interference fringes. Mirrors 1 and 2 are used to make the two incident angle detection beams return to their original path after grating diffraction to allow the Zygo interferometer to detect the wavefront and the interference fringes of the grating. The key parameters for all components are listed in Table 1. In the experiment, the peak-to-valley (PV) wavefronts of the mosaic grating elements are  $0.349\lambda$  and  $0.395\lambda$ , respectively. The incident angle  $\alpha_1$  is  $68^\circ$ , the diffraction angle  $\beta_1$  is

**Table 1**  
Key parameters for all components.

Components	Parameters	Performance index
Zygo interferometer	Wavelength Beam diameter Type	632.8 nm 100 mm GPI XP/D
Mirror	Diameter Reflectivity Root-Mean-Square (RMS)	100 mm >90% $0.005\lambda(\lambda=632.8 \text{ nm})$
Prism	Material Pass light area Wedge angle	quartz $50 \text{ mm} \times 50 \text{ mm}$ $14^\circ$
Mosaic grating element	Area Groove density Blaze angle	$35 \text{ mm} \times 35 \text{ mm}$ 79line/mm $64^\circ$
Mosaic device	Rotation accuracy Translation accuracy	0.3μrad 1nm

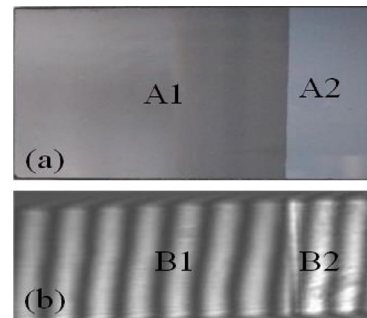


**Fig. 3.** (a) Mosaic grating element; (b) interference fringes of the mosaic grating element obtained by the Zygo interferometer. A1 is the grating area, A2 is the aluminum film area that is reserved at the edge of the grating, B1 shows the interference fringes in area A1, and B2 shows the interference fringes in area A2.

$60.75^\circ$ , the incident angle  $\alpha_2$  is  $74.66^\circ$ , and the diffraction angle  $\beta_2$  is  $56.65^\circ$

#### 3.2. Correction of initial errors of $\Delta\theta_x$ and $\Delta z$

Eqs. (5) and (6) indicate that the initial values of  $\Delta\theta_x$  and  $\Delta z$  need to be adjusted to be within a specific range before the mosaic errors are corrected. Additionally, according to the relationships between the mosaic error and the diffraction wavefronts, the zero-order diffraction light of the grating can be used to realize detection and correction of  $\Delta\theta_x$  and  $\Delta z$ . However, the detection and correction of  $\Delta\theta_x$  and  $\Delta z$  cannot be realized using the zero-order diffraction light of the grating when mosaicking echelle gratings, because the zero-order diffraction light of the echelle grating is weak.

During grating engraving, a specific area of the aluminum film is usually reserved at the grating edge to protect the grating engraving quality and to protect the diamond engraving tool. Therefore, we propose to use the light reflected by the aluminum film on the edge of the grating rather than the zero-order diffraction light of the grating at the same angle of incidence to detect and correct the initial errors of  $\Delta\theta_x$  and  $\Delta z$ . The width of the aluminum film along the grating groove direction (the long side direction of the grating) is defined as 10 mm, which can be used to complete correction of the initial error.

Fig. 3(a) shows the mosaic grating element. Area A1 is the grating area and area A2 is the reserved area of the aluminum film at the edge of the grating. Fig. 3(b) shows the interference fringes of the mosaic grating element obtained by the Zygo interferometer. In addition, correction of the initial value of  $\Delta\theta_x$  is realized by adjusting the width of the interference fringes in the aluminum film areas and correction of

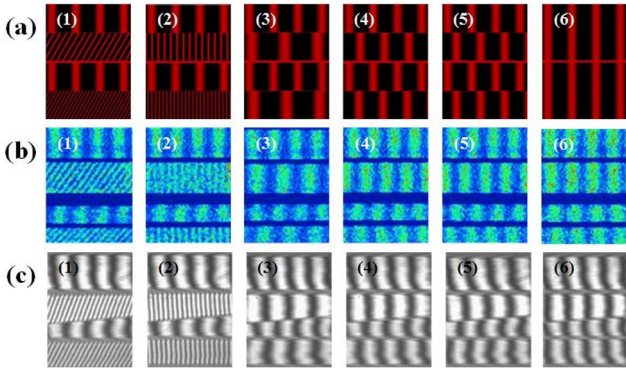


**Fig. 4.** Correction process for mosaic errors based on interference fringes of mosaic gratings. (a) Simulated results when using MATLAB, (b) simulated results when using ZWMAX software, and (c) experimental results. The correction of  $\Delta\theta_y$  is from (1) to (2); the correction of  $\Delta\theta_x$  is from (2) to (3); the correction of  $\Delta\theta_z$  is from (3) to (4); the correction of  $\Delta z$  is from (4) to (5); and the correction of  $\Delta x$  is from (5) to (6).

**Table 2**  
Mosaic errors corresponding to the mosaic errors correction process in Fig. 4.

	$\Delta\theta_x$ ( $\mu\text{rad}$ )	$\Delta\theta_y$ ( $\mu\text{rad}$ )	$\Delta\theta_z$ ( $\mu\text{rad}$ )	$\Delta x$ ( $\mu\text{m}$ )	$\Delta z$ ( $\mu\text{m}$ )
Fig.4-1	5.330	43.633	26.180	23.560	1.490
Fig.4-2	5.330	0	26.180	23.560	1.490
Fig.4-3	0	0	-4.800	14.997	1.490
Fig.4-4	0	0	0	14.997	1.490
Fig.4-5	0	0	0	14.997	0
Fig.4-6	0	0	0	0	0

the initial value of  $\Delta z$  is realized by adjusting the displacement of the interference fringes in the aluminum film areas.

According to Eqs. (5) and (6), the initial values of  $\Delta\theta_x$  and  $\Delta z$  are less than or equal to  $46.64 \mu\text{rad}$  and  $6.47 \mu\text{m}$ , respectively. Finally, these initial values of  $\Delta\theta_x$  and  $\Delta z$  are corrected to values of  $5.33 \mu\text{rad}$  and  $1.49 \mu\text{m}$ , respectively.

#### 4. Results and discussion

##### 4.1. Interference fringe adjustment process

Fig. 4 shows the correction process for mosaic errors based on the interference fringes of mosaic gratings. In each interference fringe pattern, the first row is the interference fringe of a static grating in the  $\alpha_1$  interference field, the second row is the interference fringe of the moving grating in the  $\alpha_1$  interference field, the third row is the interference fringe of the static grating in the  $\alpha_2$  interference field, and the fourth row is the interference fringe of the moving grating in the  $\alpha_2$  interference field. In addition, the values of mosaic errors corresponding to the mosaic errors correction process obtained by simulation in Fig. 4 are listed in Table 2.

From Fig. 4, the specific correction steps for mosaic errors based on the interference fringes are determined as follows:

- (1) To ensure correction accuracy for the mosaic error, the interference fringes of the static grating in the  $\alpha_1$  and  $\alpha_2$  interference fields are adjusted to be parallel and uniform in width before the mosaic error is corrected, as shown in Fig. 4(a)-1, Fig. 4(b)-1 and Fig. 4(c)-1;
- (2)  $\Delta\theta_y$  is corrected by adjusting the interference fringes of the moving grating and the static grating in the  $\alpha_1$  or  $\alpha_2$  interference fields to be parallel, as shown in Fig. 4(a)-2, Fig. 4(b)-2 and Fig. 4(c)-2;
- (3)  $\Delta\theta_x$  is corrected by adjusting the widths of the interference fringes of the moving grating in the  $\alpha_1$  and  $\alpha_2$  interference fields to be equal, as shown in Fig. 4(a)-3, Fig. 4(b)-3 and Fig. 4(c)-3. Here, the number of the interference fringes of the moving grating is usually adjusted

to about the same as the number of the interference fringes of the static grating in order to improve the accuracy of error correction, as shown in Table 2, the errors of  $\Delta\theta_z$  and  $\Delta x$  were changed from Fig. 4-2 to Fig. 4-3;

- (4)  $\Delta\theta_z$  is corrected by adjusting the widths of the interference fringes of the moving grating and the static grating in the  $\alpha_1$  or  $\alpha_2$  interference fields to be equal, as shown in Fig. 4(a)-4, Fig. 4(b)-4 and Fig. 4(c)-4;
- (5)  $\Delta z$  is corrected by adjusting the displacements of the interference fringes of the moving grating in the  $\alpha_1$  and  $\alpha_2$  interference fields to be equal, as shown in Fig. 4(a)-5, Fig. 4(b)-5 and Fig. 4(c)-5;
- (6)  $\Delta x$  is corrected by adjusting the displacements of the interference fringes of the moving grating and the static grating in the  $\alpha_1$  or  $\alpha_2$  interference fields to be equal, as shown in Fig. 4(a)-6, Fig. 4(b)-6 and Fig. 4(c)-6.

##### 4.2. Error analysis in mosaic error detection system

In the mosaic error detection system, the mosaic error between gratings is indirectly measured by the difference between the interference fringes of the mosaic gratings obtained in real time by the Zygo interferometer. The influence factors of relative measurement of mosaic errors mainly come from the surface-shape error of the mirror, the surface-shape error of the prism and the surface-shape difference between mosaic gratings. These errors mainly cause the deformation of the interference fringes of the mosaic gratings obtained by the Zygo interferometer, and then affect the detection and correction of mosaic errors, as the experimental results in Fig. 4 show the aberration when compared with the simulated results. Among them, the surface-shape error of the mirror affects the interference fringes in the  $\alpha_1$  and  $\alpha_2$  interference fields. The surface-shape error of the prism affects the interference fringes in the  $\alpha_2$  interference fields as shown in the difference between the third and first rows interference fringes or the difference between the fourth and second rows interference fringes in Fig. 4(c). The surface-shape difference between the mosaic gratings affects the interference fringes in the  $\alpha_1$  and  $\alpha_2$  interference fields as shown in the difference between the first and second rows interference fringes or the difference between the third and fourth rows interference fringes in Fig. 4(c). However, in the experiment, the surface-shape error (RMS) of the mirror is usually required to be better than  $0.005\lambda$ , the surface-shape error of the prism is required to be better than  $0.01\lambda$ , and the mosaic gratings come from the same master grating to ensure that the surface shapes of mosaic gratings are consistent with each other. Therefore, these errors have a little influence on the relative measurement of mosaic errors.

In addition to the influence of the above system errors, the detection and correction of mosaic errors are also affected by the environmental vibration. The vibration of the environment mainly causes the violent vibration of the interference fringes of mosaic gratings obtained by the Zygo interferometer, and then affects the mosaic error cannot be detected and corrected. Therefore, in the experiment, the air floating platform is also required to be used in order to eliminate the influence of environmental vibration.

##### 4.3. Standard uncertainty in wavefront detection

The PV wavefront and the root-mean-square (RMS) wavefront of the mosaic grating are measured using the Zygo interferometer. To estimate the uncertainty in this measurement, we need to calculate the Zygo interferometer measurement uncertainty and measurement repeatability. The 36th-order diffraction wavefront data of the mosaic grating are listed in Table 3, where the unit is  $\lambda$  ( $\lambda=632.8 \text{ nm}$ ).

###### (1) Zygo interferometer measurement uncertainty

The wavefront measurement accuracy of the Zygo interferometer is better than  $0.001\lambda$ . Based on a uniform distribution, the wavefront standard uncertainty caused by the Zygo interferometer's measurement er-

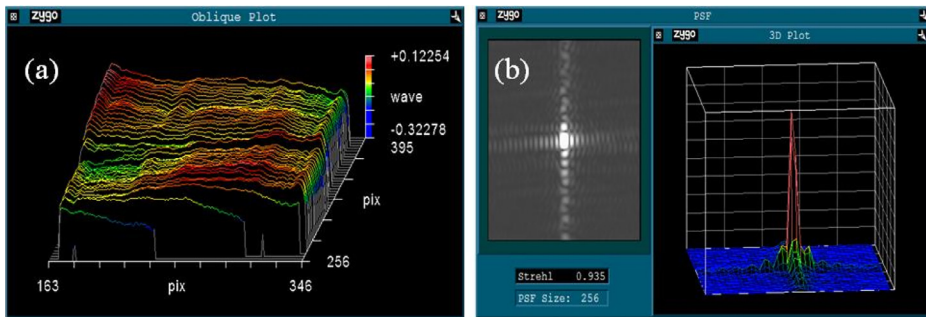


**Fig. 5.** Mosaic results obtained via the Zygo interferometer. (a) Three-dimensional wavefront of the mosaic grating; (b) Point spread function (PSF) of the mosaic grating, where the Strehl ratio is 0.935.

**Table 3**  
Wavefront data of mosaic gratings.

Mosaic grating							
PV	0.483	0.423	0.424	0.438	0.447	0.445	0.428
RMS	0.047	0.047	0.047	0.046	0.046	0.046	0.047

rror  $u_1$  can be described by the following type B uncertainty:

$$u_1 = \frac{0.001\lambda}{\sqrt{3}} = 0.0006\lambda \quad (7)$$

#### (2) Measurement repeatability

During wavefront measurement of the mosaic grating, the wavefront values are recorded seven times, and these values have been averaged to give the final results. The standard deviation of a single measurement  $\sigma$  is  $0.0208\lambda$ , and thus the wavefront standard uncertainty caused by the measurement repeatability  $u_2$  can be described by the following type A uncertainty:

$$u_2 = \frac{\sigma}{\sqrt{n}} = \frac{0.0208\lambda}{\sqrt{7}} = 0.0079\lambda \quad (8)$$

Therefore, the wavefront measurement standard uncertainty  $u$  can be expressed as a root sum square of the two errors as:

$$u = \sqrt{u_1^2 + u_2^2} = 0.008\lambda \quad (9)$$

This uncertainty is sufficiently small and can result in high-precision measurement of the grating wavefront.

#### 4.4. Mosaic accuracy of grating wavefront

The average value of the wavefront data of the mosaic gratings given in Table 3 is regarded as the final mosaic result. The average value of the PV wavefront is  $0.441\lambda$ , while the average value of the RMS wavefront is  $0.047\lambda$ .

$\Delta PV$  is defined as the difference between the mosaic grating wavefront and the average wavefront of the mosaic grating element.  $\Delta PV$  represents the mosaic accuracy of the grating wavefront. The mosaic grating meets the mosaic requirement when  $\Delta PV$  is less than  $0.2\lambda$ . The average PV of the mosaic grating element is  $0.372\lambda$  in the experiment. Therefore, the mosaic accuracy of the grating wavefront is  $0.069\lambda$  based on the mosaic method presented in this paper.

The three-dimensional data of the 36th-order diffraction wavefront of the mosaic grating were also obtained using the Zygo interferometer, as shown in Fig. 5(a). The point spread function (PSF) of the mosaic grating is also obtained via that Zygo interferometer, as shown in Fig. 5(b). The PSF shows that the diffracted energy is concentrated at the center spot. The Strehl ratio is defined as the ratio of the peak intensity of an aberrated system to the corresponding intensity of a diffraction-limited system. The Strehl ratio is 0.935 in this case.

## 5. Summary

This study presented a new method for separation detection and correction of mosaic errors based on use of detection beams of the same diffraction order but with different incident angles. This method solves the problem where the interferometer cannot detect the zero-order wavefront of an echelle grating because of the weak zero-order diffraction light, which means that the zero-order and non-zero-order diffraction light of the echelle grating cannot be used to complete separation detection and correction of mosaic errors. The proposed method is suitable for mosaics of all blazed gratings.

In the experiments, we designed and built a mosaic error separation detection system based on this method. The interference fringes of the mosaic gratings in the  $\alpha 1$  and  $\alpha 2$  interference fields can appear on the same detector simultaneously to improve the mosaic accuracy of the wavefront using this detection system. The results of mosaic experiment show that the wavefront measurement uncertainty of  $0.008\lambda$  and the wavefront mosaic accuracy of  $0.069\lambda$  can be achieved using this detection system. In addition, we summarize the correction steps for mosaic errors and analyze the error in mosaic error detection system.

## Declaration of Competing Interest

The authors declare no conflicts of interest.

## CRediT authorship contribution statement

**Guojun Yang:** Conceptualization, Methodology, Validation, Investigation, Data curation, Writing - original draft, Writing - review & editing, Visualization. **Xiangdong Qi:** Conceptualization, Resources, Supervision. **Xiaotao Mi:** Conceptualization, Writing - review & editing, Funding acquisition. **Shanwen Zhang:** Funding acquisition. **Hongzhu Yu:** Resources. **Haili Yu:** Resources. **Xiaotian Li:** Funding acquisition.

## Acknowledgments

The authors acknowledge supports from National Key R&D Program of China (2016YFF0102006); National Natural Science Foundation of China (NSFC) (61975255, 61605204, 61505204); Key Technological Research Project of Jilin Province (20190302047GX); Bethune Medical Engineering and Instrument Center Project (BQEGCZX2019017); National Youth Program Foundation of China (61805233); Jilin Province Outstanding Youth Project in China (201805020190JH); Jilin Province Science and Technology Development Plan Project (20180201035GX, 20200404197YY); Special Fund Project of High-Tech Industrialization of Science and Technology Cooperation between Jilin Province and Chinese Academy of Sciences (2018SYHZ0014).

## References

- [1] Talghader JJ, Gawarikar AS, Shea RP. Spectral selectivity in infrared thermal detection. *Light Sci Appl* 2012;1(8):e24.

- [2] Jacob R, Aaron B, Kevin P, Jannick P. Freedom spectrometer enabling increased compactness. *Light Sci Appl* 2017;6:1–10.
- [3] Qiu J, Qi X, Li X, Tang Y, Lantu J, Mi X, Bayan H. Broadband transmission Raman measurements using a field-widened spatial heterodyne Raman spectrometer with mosaic grating structure. *Opt Express* 2018;26(20):106–19.
- [4] Breitkopf S, Eidam T, Klenke A, Von L, Carstens H, Holzberger S, Fill E, Schreiber T, Krausz F, Tunnermann A, Pupeza I, Limpert J. A concept for multiterawatt fibre lasers based on coherent pulse stacking in passive cavities. *Light Sci Appl* 2014;3:e211.
- [5] Mhibik O, Forget S, Ott D, Venus G, Diviliansky I, Glebov L, Chenais S. An ultra-narrow linewidth solution-processed organic laser. *Light Sci Appl* 2016;5:e16026.
- [6] Blanchot N, Bar E, Behar G, Bellet C, Bigourd D, Boubault F, Chappuis C, Coic H, Damiens-Dupont C, Flour O, Hartmann O, Hilsz L, Hugonnot E, Lavastre E, Luce J, Mazataud E, Neauport J, Noailles S, Remy B, Sautarel F, Sautet M, Rouyer C. Experimental demonstration of a synthetic aperture compression scheme for multi-Petawatt high-energy lasers. *Opt Express* 2010;18(10):10088–97.
- [7] Schumann M, Bielunans T, Gruhler N, Wegener M, Pernice W. Hybrid 2D–3D optical devices for integrated optics by direct laser writing. *Light Sci Appl* 2014;3(6):e175.
- [8] Logan S, Rahul T, Sapra NV, Piggot AY, Vercruyse D, Vuckovic J. Fully-automated optimization of grating couplers. *Opt Express* 2018;26(4):4023–34.
- [9] Ghulam SM, Wang Y, Eslam EF, David P, Arif SK, Samiul AM, Maxime J, Xing ZP, Xu L, Nicolas A, David P. Transversely coupled Fabry–Perot resonators with Bragg grating reflectors. *Opt Lett* 2018;43(1):13–16.
- [10] Szentgyorgyi A, Baldwin D, Barnes S, Bean J, Ben-Ami S, Brennan P, Budynkiewicz J, Chun MY, Conroy C, Crane JD, Epps H, Evans I, Evans J, Foster J, Frebel A, Gauron T, Guzmán D, Hare T, Jang BH, Jang JG, Jordan A, Kim J, Kim KM, Oliveira CMM, Lopez-Morales M, McCracken K, McMullroch S, Miller J, Mueller M, Oh JS, Onyuksel C, Ordway M, Park BG, Park C, Park SJ, Paxson C, Phillips D, Plummer D, Podgorski W, Seifahrt A, Stark D, Steiner J, Uomoto A, Walsworth R, Yu YS. The GMT-Consortium Large Earth Finder (G-CLEF): an optical Echelle spectrograph for the Giant Magellan Telescope (GMT). *Proc SPIE* 2016;9908:990822.
- [11] Lizon JL, Dekker H, Manescu A, Megevan D, Pepe FA, Riva M. A large mosaic echelle grating for ESPRESSO spectrograph. *Proc SPIE* 2018;10701:107012P.
- [12] Maywar DN, Kelly JH, Waxer LJ, Morse SFB, Begishev IA, Bromage J, Dorrer C, Edwards JL, Folnsbee L, Guardalben MJ, Jacobs SD, Jungquist R, Kessler TJ, Kidder RW, Kruschwitz BE, Loucks SJ, Marcante JR, McCrory RL, Meyerhofer DD, Okishev AV, Oliver JB, Pien G, Qiao J, Putth J, Rigatti AL, Schmid AW, Shoup MJ III, Stoeckl C, Thorp KA, Zuegel JD. OMEGA EP high-energy petawatt laser: progress and prospects. *J Phys Conf Ser* 2008;112(3):32007.
- [13] Neauport J, Bonod N. Pulse compression gratings for the PETAL project a review of various technologies. *Proc SPIE* 2009;7132:71320D.
- [14] Yang X, Xia L, Ma W, Dai Y. Experiment of real-time monitoring and adjusting of rotation error about tiled gratings. *Chin J Laser* 2007;34(9):1222–6.
- [15] Zeng L, Li L. Method of making mosaic gratings by using two-color heterodyne interferometer containing a reference grating. *Opt Lett* 2006;31(2):152–4.
- [16] Hu Y, Zeng L. Grating mosaic based on image processing of far-field diffraction intensity patterns in two wavelengths. *Appl Opt* 2007;46(28):7018–25.
- [17] Hu Y, Zeng L, Li L. Method to mosaic gratings that relies on analysis of far-field intensity patterns in two wavelengths. *Opt Commun* 2007;269(2):285–90.
- [18] Qiao J, Kalb A, Guardalben M, King G, Canning D, Kelly J. Large-aperture grating tiling by interferometry for petawatt chirped-pulse-amplification systems. *Opt Express* 2007;15:9562–74.
- [19] Lu Y, Qi X, Li X, Yu H, Jiang S, Bayan H, Yin L. Removal of all mosaic grating errors in a single-interferometer system by a phase-difference reference window. *Appl Opt* 2016;55:7997–8002.
- [20] Cong M, Qi X, Mi X, Bayan H. Interference method for mosaicking echelles using double-angle incident light and a mirror-echelle structure. *Opt Eng* 2018;57(6):064111.
- [21] Cong M, Qi X, Xu J, Qiao C, Mi X, Li X, Yu H, Zhang S, Yu H, Bayan HSG. Analysis and removal of five-dimensional mosaicking errors in mosaic grating. *Opt Express* 2019;27(3):1968–80.